chemosensors

MDPI

Article

Metallo-Liposomes Derived from the $[Ru(bpy)_3]^{2+}$ Complex as Nanocarriers of Therapeutic Agents

Maria Luisa Moyá [1], Francisco José Ostos [1], Izamar Moreno [1], Diandra García [1], Paula Moreno-Gordillo [2], Ivan V. Rosado [2], Pilar López-Cornejo [1,*], José Antonio Lebrón [1,*] and Manuel López-López [3,*]

1 Department of Physical Chemistry, Faculty of Chemistry, University of Seville, C/Professor García González 1, 41012 Seville, Spain; moya@us.es (M.L.M.); fostos@us.es (F.J.O.); izamar82moreno@gmail.com (I.M.); diandraa95@gmail.com (D.G.)
2 Institute of Biomedicine of Seville (IBiS), University Hospital Virgen del Rocio/CSIC/University of Seville, Avda. Manuel Siurot s/n, 41013 Seville, Spain; paulamorenog95@gmail.com (P.M.-G.); ivrosado@us.es (I.V.R.)
3 Department of Chemical Engineering, Physical Chemistry and Materials Science, Faculty of Experimental Sciences, Campus de El Carmen, Avda. de las Fuerzas Armadas s/n, 21071 Huelva, Spain
* Correspondence: pcornejo@us.es (P.L.-C.); jlebron@us.es (J.A.L.); manuel.lopez@diq.uhu.es (M.L.-L.)

Abstract: The obtaining of nanocarriers of gene material and small drugs is still an interesting research line. Side-effects produced by the toxicity of several pharmaceutics, the high concentrations needed to get therapeutic effects, or their excessive use by patients have motivated the search for new nanostructures. For these reasons, cationic metallo-liposomes composed by phosphatidylcholine (PC), cholesterol (CHO) and RuC1C19 (a surfactant derived from the metallic complex $[Ru(bpy)_3]^{2+}$) were prepared and characterized by using diverse techniques (zeta potential, dynamic light scattering and electronic transmission microscopy –TEM-). Unimodal or bimodal populations of spherical aggregates with small sizes were obtained depending on the composition of the liposomes. The presence of cholesterol favored the formation of small aggregates. ct-DNA was condensed in the presence of the liposomes investigated. In-vitro assays demonstrated the ability of these nanoaggregates to internalize into different cell lines. A positive gene transfection into human bone osteosarcoma epithelial cells (U2OS) was also observed. The RuC1C19 surfactant was used as sensor to quantify the binding of DNA to the liposomes. Doxorubicin was encapsulated into the metallo-liposomes, demonstrating their ability to be also used as nanocarriers of drugs. A relationship between then encapsulation percentage of the antibiotic and the composition of the aggregates has been established.

Keywords: metallo-liposome; nanocarrier; gene therapy; DNA; doxorubicin; TEM; sensor

Citation: Moyá, M.L.; Ostos, F.J.; Moreno, I.; García, D.; Moreno-Gordillo, P.; V. Rosado, I.; López-Cornejo, P.; Lebrón, J.A.; López-López, M. Metallo-Liposomes Derived from the $[Ru(bpy)_3]^{2+}$ Complex as Nanocarriers of Therapeutic Agents. *Chemosensors* **2021**, *9*, 90. https://doi.org/10.3390/chemosensors9050090

Academic Editor: Nicole Jaffrezic-Renault

Received: 12 March 2021
Accepted: 19 April 2021
Published: 25 April 2021

1. Introduction

Metallosurfactants are amphiphilic molecules containing metal ions anchored in their structure. The metal ion is usually located at the head group of the molecule [1,2], although it can also be found in the hydrophobic tail [3,4] or acting as counter ion of the polar head group [5,6]. The presence of a metal ion in the surfactant confers the molecule characteristic properties for applications such as catalyst in heterogeneous processes or electron storage devices in photoredox processes. Metallosurfactants have also been used as potential precursors in new synthetic methods, as antimicrobial and antibactericidal agents, and as contrast agents in diagnostic tests, etc. [7–10].

The amphiphilic character of surfactants favors the formation of diverse nanostructures such as micelles or liposomes. The use of these assemblies as nanovehicles of drugs has become an important work line for numerous researchers in recent decades [11–14]. Genetic material, antibiotics or antineoplastic agents, among others, have been encapsulated into these structures to improve their delivery into the target cells, to reduce their side effects or to enhance their activity [15,16].

The incorporation of metal ions into these nanostructures has improved the transfection processes of several nanocarriers [17] and has also showed a decrease in the energy

status in tumor cells that provokes the deactivation of the cell functions and their subsequent death [18]. Metallo-surfactants of Fe(II), Ni(II), Co(II) and Cu(II) are able to provoke changes in the primary and/or secondary structures of the bovine serum albumin protein, BSA, depending on the type of assembly formed [19]. Recently, building blocks of calix [4] resorcinol and a lanthanum-based surfactant have been prepared for encapsulating the anticancer drug cisplatin [20]. Results showed an increase of the toxicity of the drug to HeLa cells and a decrease to normal Chang liver cells. This selective activity of cisplatin towards cancer cells seems to be an important research line to diminish strong side effects provoked by this drug in cancer treatments. Multifunctional metallo-organic fluorescent vesicles have also been prepared as cell imaging agents, nanocarriers of anticancer drugs and metal ions detection [21].

With respect to the use of metallosurfactants in the preparation of liposomes, several metalloliposomes (also known as metallosomes or metallovesicles) have been synthesized. Liposomes containing Cu(II) metallosurfactants of 1-alkyl-1,4,7-triazaclononane with different hydrocarbon tail lengths were prepared to condense pEGFP-N1 plasmids and be used as vectors with a good transfection efficiency [22]. On the contrary, the use of the bis-(4-pyridylmethyl hexadecanoate)-(1,4,7-triazacyclononane) copper(II) metallosurfactant showed low or even zero transfection efficiency [23]. Cruz-Campa [24] et al. studied the transfection process of liposomes with analogues metallosurfactants containing the same hydrocarbon tail, but different metal ions in the polar head groups. Results reported similar values for gene transfection in in-vitro assays; no dependence on the nature of the metal was observed.

Recently, unilamellar liposomes of DOPE (1,2-dioleoyl-sn-glycero-3-phosphoethanolamine) and metallosurfactant molecules derived from the $[Ru(bpy)_3]^{2+}$ complex, with two different hydrocarbon tail lengths, were synthesized by our group [25]. Strong interaction with DNA, low toxicity and good internalization into cells were observed for different cell lines. However, the transfection efficiency obtained was low, although slightly higher for the liposomes containing metallosurfactant molecules with longer hydrocarbon tails.

It is important to emphasize the multifunctional ability provided by the liposome structure. The presence of hydrophobic and hydrophilic areas in the same assembly allows for the encapsulation of more than one drug, and also drugs with different hidrophobic character. This can produce synergetic effects that improve treatments of some diseases [26–28].

Despite the known antitumor and antimetastatic properties of some ruthenium complexes [29,30], few studies with liposomes containing ruthenium-based surfactants are found in the literature to date. Bearing this in mind and with the aim of searching for effective non-viral vectors in gene therapy, new metallo-liposomes have been prepared by using l-α-phosphatidylcholine (PC) from egg yolk, cholesterol (CHO) and the single-chained metallosurfactant derived from the $[Ru(bpy)_3]^{2+}$ complex $[Ru(2,2'\text{-bipy})_2(4\text{-}(CH_3)\text{-}4'\text{-}(C_{19}H_{39})\text{-}2,2'\text{-bipy})]Cl_2$ (RuC1C19). The $[Ru(bpy)_3]^{2+}$ complex was chosen as the polar head group due to its photochemical properties, which allows using the metallosurfactant as biosensor to obtain information about the system, including internalization processes into cells, without the addition of another agent that can provoke changes in the structurers of the nanoaggregates and in their interaction with other molecules.

The structural characteristics of this Ru metalloliposomes permits encapsulating a diverse pharmaceutical agent. This was exploited to encapsulate doxorubicin and DNA.

The structures of both the different lipids and the surfactant used in the preparation of the metallo-liposomes are shown in Figure 1.

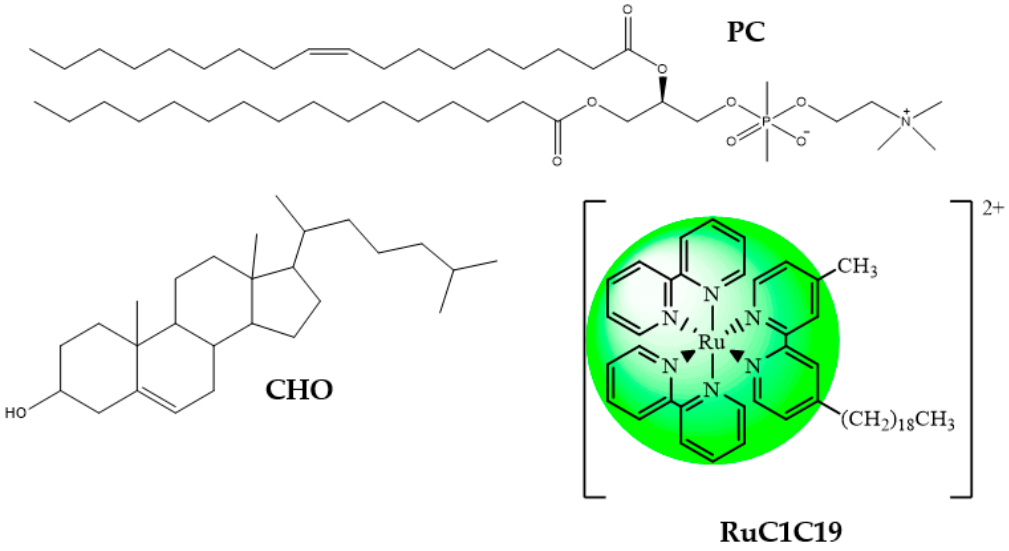

Figure 1. Structures of both the lipids and the surfactant used in the preparation of the metallo-liposomes.

2. Materials and Methods

2.1. Materials

Calf thymus DNA (ct-DNA), L-α-phosphatidylcholine (PC) from egg yolk, cholesterol (CHO) and doxorubicin (DOX) were purchased from Sigma-Aldrich. The structures of the lipids, the surfactant and the drug used in the preparation of the metallo-liposomes are shown in Figures 1 and 2. All reagents were of analytical grade (P.A.) and used without further purification.

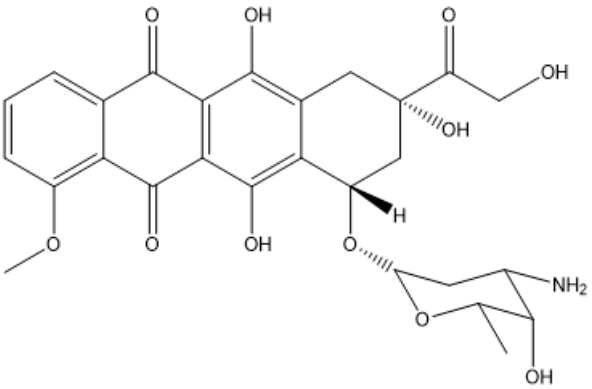

Figure 2. Doxorubicin.

The concentration of the polynucleotide, given by phosphate groups, was determined spectrophotometrically. A molar absorption data of 6600 mol^{-1} dm^3 cm^{-1} at 260 nm was used to calculate the DNA concentration. The molar absorbance ratios of the solutions A260 nm/A280 nm observed were in the range of 1.7–1.8. This suggests the absence of proteins in the solutions. An average number of base pairs per DNA molecule of 10,000 bp was obtained by using agarose gel electrophoresis using ethidium bromide.

All solutions were prepared with distilled and deionized water from a Millipore Milli-Q system (Darmstadt, Germany) with a conductivity value lower than 10^{-6} S m^{-1}. The pH of the solutions was maintained constant at a value of 7.4 with a HEPES buffer (I = 0.01 mol·dm^{-3}). All the measurements were done at 298.0 ± 0.1 K.

The synthesis of the ruthenium surfactant [Ru(2,2′-bipy)$_2$(4-CH_3,4′-($C_{19}H_{39}$)-2,2′-bipy)]Cl_2 (RuC1C19, see Figure 1) was described in a previous paper [31]. Its characterization was carried out by using IR and NMR spectra, as well as by elemental analysis

(C, H, N): 1H NMR (CD_3OD): δ 0.80 (t, JHH = 6.9 Hz, 3H,$CH_2CH_2(CH_2)_{16}CH_3$), 1.18 (m Br, 32H, $CH_2CH_2(CH_2)_{16}CH_3$), 1.65 (q, JHH = 7.2 Hz, 2H, $CH_2CH_2(CH_2)_{16}CH_3$), 2.56 (s, 3H, CH_3), 2.79 (t, JHH = 7.7 Hz, 2H, $CH_2CH_2(CH_2)_{16}CH_3$), 7.25 (t, JHH = 5.9 Hz, 2H, 5,5′-CH of alkyl-substituted bipy), 7.46 (m, 4H, 5,5′-CH of bipy), 7.62 (m, 2H, 6,6′-CH of alkyl-substituted bipy), 7.64 (t, JHH = 5.3 Hz, 4H, 4,4′-CH of bipy), 8.06 (m, 4H, 6,6′-CH of bipy), 8.59 (s, 2H, 3,3′-CH of alkylsubstituted bipy), 9.07 (d, JHH = 7.9 Hz, 4H, 3,3′-CH of bipy). 13C{1H}NMR (CD3OD): δ 14.6 (s, $CH_2CH_2CH_2(CH_2)_{13}CH_2CH_2CH_3$), 20.5 (s, $CH_2CH_2CH_2(CH_2)_{13}CH_2CH_2CH_3$), 22.6 (s, $CH_2CH_2CH_2(CH_2)_{13}CH_2CH_2CH_3$), 32.1–32.5 (several s, $CH_2CH_2CH_2(CH_2)_{13}CH_2CH_2CH_3$), 34.2 (s, $CH_2CH_2CH_2(CH_2)_{13}CH_2CH_2CH_3$), 36.5 (s, $CH_2CH_2CH_2(CH_2)_{13}CH_2CH_2CH_3$), 54.3 (s, $CH_2CH_2CH_2(CH_2)_{13}CH_2CH_2CH_3$), 125.0–131.2 (several s, 3,3′ or 5,5′-CH of bipy), 140.9 (s, 4,4′-CH of bipy), 153.2–160.1 (several s, 2,2′ or 6,6′-CH of bipy). Elemental analysis for $C_{50}H_{64}Cl_2N_6Ru$: calc.: C, 49.1; H, 4.71; N, 8.18, Experimental: C, 49.3; H, 4.69; N, 8.14. ESI-MS in positive ion mode: found m/z 851.43 for [RuC1C19+1]+, calculated for C50H64N6Ru, 850.42.

All these measurements were done in the Research Services of the University of Seville (CITIUS). Results agree with those previously reported.

2.2. Liposome Formation

The lipid thin film hydration method was used in the preparation of the metallo-liposomes. Desired amounts of cholesterol, phosphatidylcholine, and the ruthenium-based surfactant RuC1C19 were dissolved in 2 mL of chloroform and sonicated for 120 s. Different quantities of lipids and surfactant were mixed to obtain the required molar fraction. The organic solvent of the mixture was evaporated using a rotary evaporator for 50 min at 310 K (human body temperature). This resulted in a dry lipid film that was stored at 193 K for at least 24 h to avoid degradation of the phospholipid. After 24 h, the lipid film was hydrated with 2 mL of a 10 mM HEPES aqueous solution (pH = 7.4) and subjected to 10 alternating cycles of vortex (3 min/1200 rpm) and sonication (2 min, JP Selecta Ultrasons system 200 W and 50 kHz). Finally, the solution was stirred for 1 h at room temperature.

The extrusion of the liposome solutions gave uniform populations of unilamellar liposomes with a homogeneous size distribution (low polydispersity). This procedure was carried out using a mini extruder from Avanti Polar Lipids and polycarbonate membranes of 100 nm diameters from Whatman. The liposome solutions were extruded 10 times. Complete stabilization of the nanosystems was achieved, keeping the solutions in darkness at 277 K for 24 h.

The composition of the cationic liposomes was expressed in molar fraction ($\boldsymbol{\alpha}$), which is defined as the molar fraction of cationic surfactant (see Equation (1)).

$$\boldsymbol{\alpha} = \frac{\mathbf{n}_+}{\mathbf{n}_+ + \mathbf{n_{PC}} + \mathbf{n_{CHO}}} \quad (1)$$

$\mathbf{n}_+$, $\mathbf{n_{PC}}$ and $\mathbf{n_{CHO}}$ being the mole number of the cationic surfactant (RuC1C19), zwitterionic lipid (PC) and neutral lipid (CHO), respectively. All concentrations are referred to the total volume of solution.

Different liposome samples were prepared, varying the mass of both the lipids and the surfactant used. The composition of the different samples is collected in Table 1. As can be seen, the mass of CHO was changing in Series 1, the PC in Series 2 and the RuC1C19 in Series 3.

Table 1. Liposome composition (mass ratio and mole ratio) and value of molar ratio (α). All values are referred to a mass of 6×10^{-4} g (or 6.51×10^{-7} mol dm^{-3}) of RuC1C19.

SERIES	SAMPLE	Mass Ratio RuC1C19:PC:CHO	Mole Ratio RuC1C19:PC:CHO	α
1	**A**	1:0.1:0.083	1:0.11:0.20	0.76
	B	1:0.1:0.83	1:0.11:1.20	0.43
	C	1:0.1:2.55	1:0.11:2.00	0.32
2	**D**	1:0.05:0.17	1:0.058:0.51	0.69
	E	1:0.3:0.17	1:0.36:0.51	0.57
	F	1:0.5:0.17	1:0.58:0.51	0.51
3	**G**	1.16:0.33:0.17	1.16:0.23:0.40	0.65
	H	0.83:0.33:0.17	0.83:0.23:0.40	0.57
	I	0.33:0.33:0.17	0.33:0.23:0.40	0.35

2.3. Lipoplex Formation

The composition of the lipoplexes (liposome/DNA complexes) can be expressed by the mass ratio L/D, defined as:

$$\frac{\mathbf{L}}{\mathbf{D}} = \frac{\textbf{total lipid mass}}{\textbf{DNA mass}} = \frac{\mathbf{Ru^{+}mass + PC\ mass + CHO\ mass}}{\textbf{DNA mass}} \quad (2)$$

where $\mathbf{Ru^{+}}$ mass is the mass of the ruthenium-based surfactant (RuC1C19). The same mass of DNA (1.0×10^{-4} g) was used in all the measurements, which corresponds to a concentration value in base pairs of 8.1×10^{-5} mol·dm^{-3}. Appropriate volumes of liposome and aqueous DNA solution were mixed to obtain the L/D required for each α value studied. All solutions are prepared in HEPES 10 mM (pH = 7.4)

2.4. Dynamic Light-Scattering Measurements (DLS)

DLS technique (Malvern, Worcestershire, UK) was used to determine the size and the polydispersity index of the different liposomes. Samples were illuminated with a laser at a fixed detection arrangement of 90° to the center of the cell area. Fluctuations in the intensities of the scattered light were analyzed. The results obtained were the average of 10 measurements. The total lipid + surfactant concentration used was 150 μg/mL.

2.5. Zeta-Potential Measurements

A Zetasizer Nano ZS Malvern Instrument Ltd. (Malver, Worcestershire, UK) was used in Zeta-potential (ζ) experiments. The electrophoretic mobility of the sample was measured from the velocity of the particles using a Laser Doppler velocimeter (LDV, (Malver, Worcestershire, UK). A DTS1060 polycarbonate capillary cell was used at 310.1 ± 0.1 K. The total lipid + surfactant concentration used was 150 μg/mL.

2.6. Electronic Transsmision Microscopy (TEM)

A Zeiss Libra 120 scanning electron microscope at 80 kV was used to record TEM images of lipoplexes. Samples were prepared by impregnation on a 300 mesh copper grid coated with collodion. Images were processed with a bottom-mounted TEM CCD camera and recorded with a resolution of 2048 × 2048 pixels. A concentration of total lipid of 150 μg/mL was used.

2.7. Emission Spectra

Emission spectra of liposomal solutions were performed in the presence and absence of DNA to quantify the interaction between DNA and the liposome; that is, to estimate the equilibrium constant of lipoplex formation. Measurements were carried out in a Hitachi F-2500 spectrofluorimeter interfaced to a PC for the recording and handling of the spectra. This apparatus was connected to a flow Lauda thermostat to maintain the temperature at 310.0 ± 0.1 K. A standard fluorescence quartz cell of 10 mm path length

was used. Emission intensities of the lipoplexes prepared (PC/CHO/RuC1C19-based liposomes + DNA) were run at α = 0.32 and different L/D values. DNA concentration used was 8.1×10^{-5} mol dm^{-3}. The excitation and emission wavelengths used were 456 nm and 600 nm, respectively.

Emission spectra were also run to obtain information about the release of DOX from liposomes in the presence and absence of DNA at different polynucleotide concentrations at human body temperature (310.1 $\pm$ 0.1 K). The excitation and emission wavelengths used were 500 nm and 538 nm, respectively. It is important to note that these measurements were carried out at λexc = 500 nm instead of 490 nm (the maximum absorbance wavelength of DOX in solution) in order to avoid an overlap of this band with that corresponding to the emission of the RuC1C19 surfactant (λem = 600 nm and λexc = 456 nm).

2.8. Circular Dichroism Spectra

Electronic circular dichroism (CD) spectra were recorded in a Biologic Mos-450 spectropolarimeter (Barcelona, Spain). Spectra of naked DNA and lipoplexes were collected at a constant α value and different L/D values. A DNA concentration of 8.1×10^{-5} mol dm^{-3} was used. Each spectrum was obtained from an average of 10 runs with a 5 min equilibration before each scan at 310.1 $\pm$ 0.1 K by using a standard quartz cell of 10 mm path length. The spectra obtained were expressed in terms of ellipticity, Θ_{obs}.

2.9. Encapsulation Efficiency Measurements

Drug encapsulation efficiency was measured using a dialysis method. 600 µL of drug-loaded liposome was added to a Sigma-Aldrich Pur-A-Lyzer Midi 1000 dialysis kit (MWCO 1 kDa). A dialysis tube with a molecular weight limit of 12 kDa (Sigma-Aldrich, St. Louis, MO, USA) was also used, and the results obtained were similar. The dialyzer was plunged into a beaker containing 30 mL of the same buffer used for liposome hydration. The liposome's stabilization was ensured, carrying out the dialysis process at 277.1 $\pm$ 0.1 K throughout all the measurements. An aliquot (1 mL) of the buffer deposited in the beaker was taken every 15 min. The quantification of loaded antibiotics was carried out by UV-vis spectroscopy (λ = 490 nm for DOX). These aliquots were replaced each time by an equal volume of buffer to keep constant the total volume of buffer in the beaker. Dialysis was continued for a period of at least 24 h. The encapsulation efficiency (EE) was obtained using Equations (3) and (4).

$$\mathbf{EE}\% = \frac{[\mathbf{Drug}]\mathbf{L}}{[\mathbf{Drug}]\mathbf{total}} \times 100 \quad (3)$$

$$[\mathbf{Drug}]_{\mathbf{L}} = [\mathbf{Drug}]_{\mathbf{total}} - [\mathbf{Drug}]_{\mathbf{buffer}} \quad (4)$$

[Drug]$_L$, **[Drug]$_{buffer}$** and **[Drug]$_{total}$** being the drug concentration encapsulated in the liposomes, the concentration in the buffer solution, and the total concentration added to the liposomes, respectively. All concentrations are referred to the same total volume. Each measurement was performed in triplicate.

2.10. In Vitro Assays

Cytotoxic activity was carried out using the MTT assay. Cell lines were plated out into 96-well plates at a density of 3000 cells per plate. The cell lines studied were: A549 (adenocarcinomic human alveolar basal epithelial cell line), HepG2 (human liver cancer cell line), LS180 (adenocarcinomic human colonic epithelial cell line), MCF7 (breast cancer cell line), RPE-1 (hTERT-immortalized retinal pigment epithelial cell line, normal cell line) and U2OS (human bone osteosarcoma epithelial cells). The assays were recorded at different doses of liposome. Liposome solutions were added to the wells and the plate returned to the incubator for three more days. Later, they were pulsed with MTS (ROCHE). Cell viability was measured by luminometry according to the manufacturer's instructions. Each dose point was measured in triplicate.

Fluorescence microscopy was used to prove the intake of the liposomes prepared in diverse cancer and normal cell lines, studying the luminescence properties of the $[Ru(bpy)_3]^{2+}$ complex. In these assays, living cells were exposed to liposome solutions of RuC1C19 for 24 h. After the incubation time, cells were repeatedly washed with a PBS solution and mounted on coverslips using Prolong antifade mounting medium (Invitrogen, Ltd., Inchinnan, Renfrewshire, Scotland). Images were taken with a DP72 camera attached to an Olympus BX61 fluorescence microscope using 40× magnification lenses, with an excitation filter at 470–490 nm and emission long-pass filter at 520 nm. Images were analysed using cellSens Dimension software.

Gene transfection assays were done in the U2OS cell line. 4×10^4 cells were seeded in 24-well plates. The plasmid pEGFP (0.5 µg) was mixed with liposomes at α = 0.32 (L/D = 11 and 110) or α = 0.69 (L/D = 8 and 80), with and without DOPE, in 100 µL of Optimem and incubated for 20 min at RT before being added to the cell cultures, and incubated for further 24 h. Upon incubation, the transfection medium was replaced by fresh DMEM (Dubelcco's modified eagle medium) and incubated for further 16 h. Transfected cells were seeded in coverslips (VWR) and incubated for 16 h before being subjected to fluorescent microscopy. Following the incubation, cells were fixed with 4% formaldehyde in PBS at 277 K for 15 min, and further permeabilized using 0.25% Triton X-100 in PBS for 15 min. Then, cells were incubated with 4′6-diamidine-2-phenylindole dihydrochloride (DAPI) (1/2000) for 15 min at RT, to stain nuclear DNA. Finally, coverslips were mounted in ProLong® Gold Antifade Reagent (Invitrogen).

3. Results and Discussion

3.1. Characterization of Metallo-Liposomes

Metallo-liposomes containing a mixing of lipids (PC and CHO) and the ruthenium-based surfactant RuC1C19 (see Figure 1) were prepared at different α molar fractions. Table 1 contains both the mass and the molar ratio of the liposomes formulated. The aggregates were characterized by using different methods. The size, polydispersity index and zeta potential values obtained for all liposomal aggregates are listed in Table 2.

Table 2. Average size, polydispersity index (PDI) and zeta potential (ζ) values obtained for all the liposomes prepared. All values are referred to a mass of 6×10^{-4} g (or 6.51×10^{-7} mol dm^{-3}) of RuC1C19. Errors represent standard deviation.

SERIES	SAMPLE	A	Size/nm	PDI	ζ/mV
1	**A**	0.76	206 ± 15	0.669	67.3 ± 3.2
	B	0.43	130 ± 10	0.0953	46.7 ± 1.6
	C	0.32	136 ± 8	0.0686	38.8 ± 1.5
2	**D**	0.69	147 ± 12	0.636	55.2 ± 2.2
	E	0.57	135 ± 15	0.262	51.4 ± 1.2
	F	0.52	146 ± 6	0.241	43.5 ± 3.0
3	**G**	0.65	128 ± 15	0.210	40.2 ± 1.2
	H	0.57	143 ± 10	0.289	48.6 ± 1.5
	I	0.35	135 ± 14	0.089	52.9 ± 0.8

Three different series of liposomes were prepared. Only the mass of one of the species was changed in each series. So, the mass of cholesterol was changed in Series 1, while the masses of PC and RuC1C19 were maintained invariant. The PC mass was changed in the Series 2 and that for RuC1C19 in the Series 3.

With respect to Series 1, an increase of the cholesterol mass (and therefore a decrease in α parameter) diminishes both the size and the polydispersity index of the liposomes. Samples B and C shows a good polydispersity index, that is, a large homogeneity in size of the liposomal solution. In fact, a unique population of liposomes with a size about 130 nm was observed (see histograms in Figure 3A). On the contrary, a high PDI value and a bimodal size distribution (see Figure 3A) are observed for the sample A, the sample with

the lowest cholesterol mass. Therefore, the presence of cholesterol molecules at the lipid bilayer seems to favor the compaction of the lipid membrane containing both the Ru(II) metallosurfactant and the PC lipid, diminishing the size of the liposomes and forming unimodal populations.

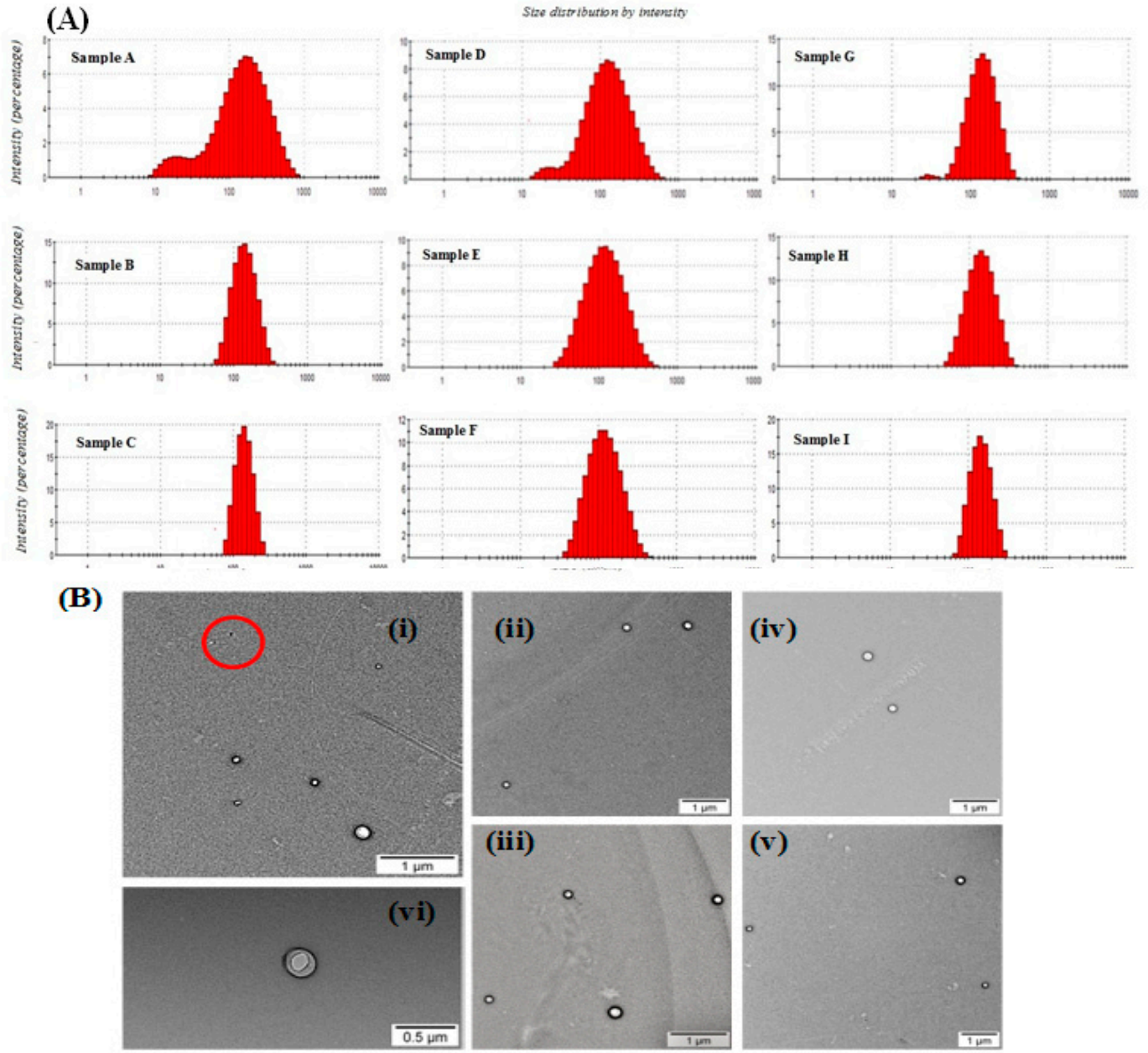

Figure 3. *Cont.*

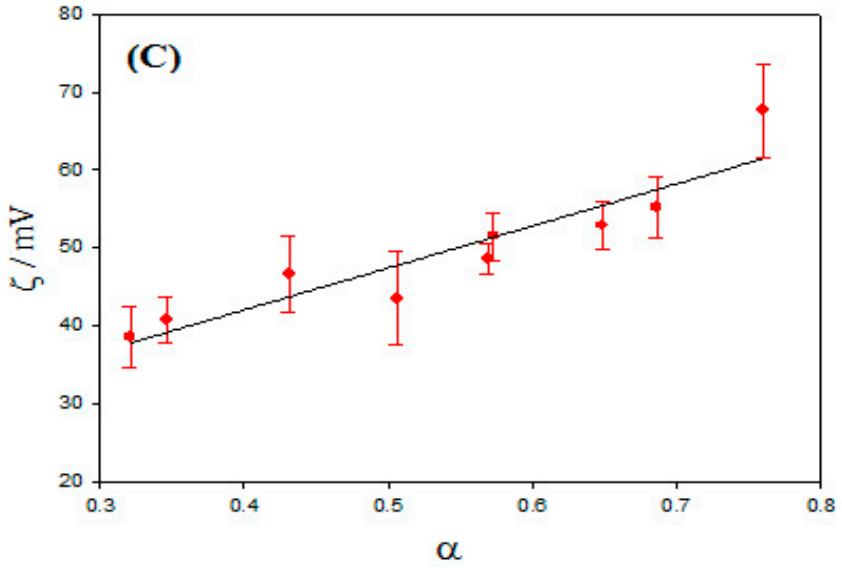

Figure 3. (**A**) Size distribution histogram of liposome samples based on dynamic light scattering measurements. (**B**) TEM images of Ru(II)-based liposomes with different α values (i: sample D magnification 3 k; ii: sample I magnification 3 k; iii: sample B magnification 4 k; iv: sample F magnification 5 k; v: sample H magnification 5 k; vi: sample C magnification 40 k). Red circle shows the micellar structure. (**C**) Plot of zeta potential values versus α values.

Similar behavior is observed in samples D (Series 2) and G (Series 3). In these cases, although the cholesterol mass used is the double than that in sample A, bimodal size distributions and a high PDI values are also observed. It must be noted that samples A, D, and G have a high α value (>0.6). Therefore, the obtaining of liposome solutions with unimodal populations does not depend on the lipid (or surfactant) concentration but on their molar fraction. The presence of different populations was also observed from TEM images (Figure 3B). This microscopy technique demonstrated the spherical structure of the liposomes prepared. The smallest population observed in samples A, D and G, with sizes about 20 nm, could correspond to the formation of micelles (or pseudomicelles) due to the presence of higher surfactant concentrations in the solution [31].

The sizes and the PDI values of the liposomes depend neither on the metallosurfactant mass nor on the PC mass for α values below 0.6.

Table 2 also contains the zeta potential values obtained for the different samples. Positive values were observed in all cases, as was expected. According to the results, ζ increases when the concentration of RuC1C19 augments and depends on neither the PC mass nor the CHO mass. This is demonstrated in Figure 3C, where a linear relationship between the zeta potential values and α parameter is observed.

It is important to have information about the toxic character of any nanosystem being used as a drug carrier. Bearing this in mind, cytotoxicity measurements of RuC1C19/PC/CHO liposomes were carried out in different cancer cell lines (MCF7, LS180, A549, U2OS and HepG2) and the normal cell line RPE-1 (Figure 4).

No differences were found for the three α studied. In general, the nanoaggregates seem to be less toxic for both the human liver carcinoma cells HepG2 and the non tumoral RPE-1 cells within the range of concentration studied. On the contrary, the cancer cell lines MCF7 and LS180 show a higher sensibility to the metallo-liposomes for equivalent doses. The A549 cells showed an intermediate situation. The adenocarcinomic human alveolar basal epithelial cells A549 seem to be less sensible than the breast adenocarcinoma MCF7 and the human colon cells LS180, but more sensible than the HepG2 and RPE-1 cell lines. The liposomes also show an acceptable viability into the cancer cell line U2OS, being something less toxic for bimodal (α = 0.69) than for unimodal (α = 0.32) populations.

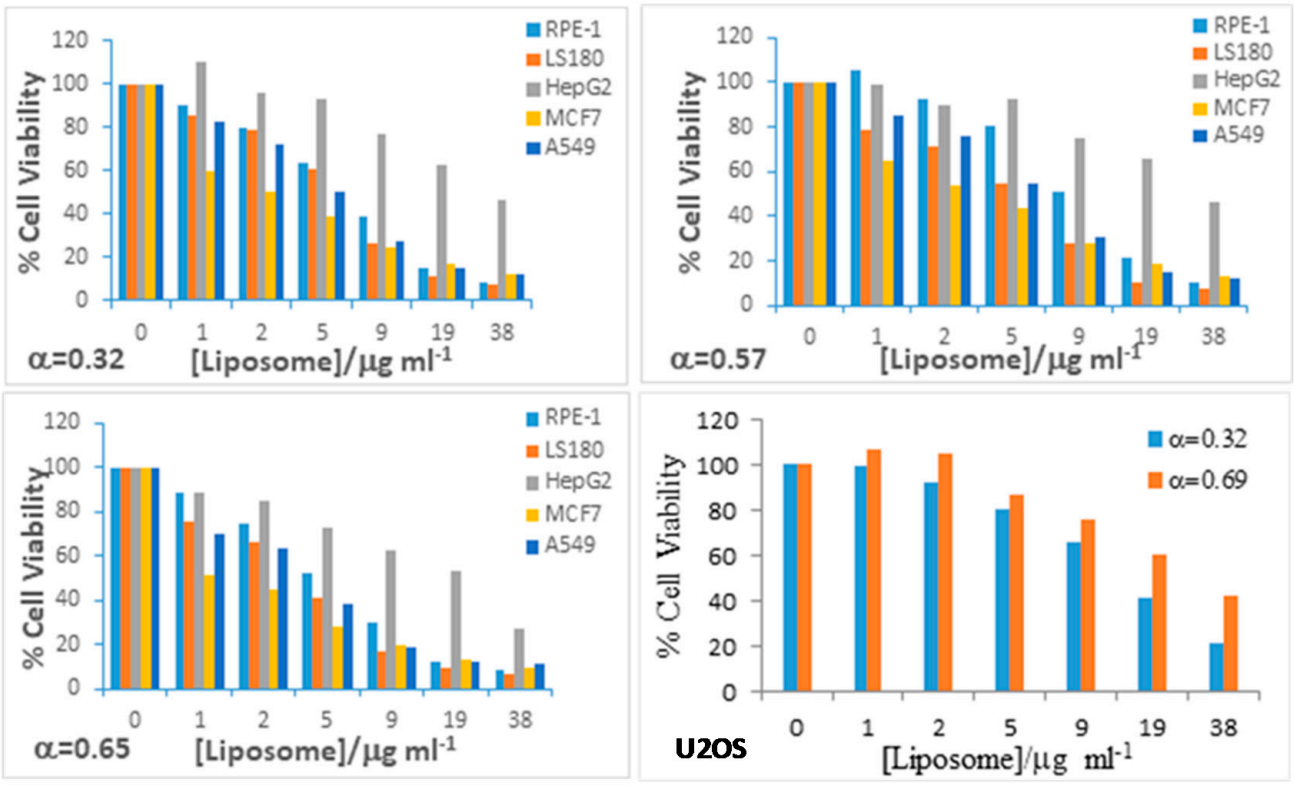

Figure 4. Cell viability of RuC1C19-based liposomes in cancer and normal cell lines at different α values and liposome concentrations.

3.2. Formation of Metallolipoplexes. Binding of Metallo-Liposomes to ct-DNA

The in-vitro study of DNA condensation is considered an important working tool whose results can be used in gene therapy. The packaged and the protection of the genetic material are processes required in this technique.

Cationic liposomes are nanomaterials able to bind to the phosphate groups of the DNA backbone by electrostatic interactions. This can provoke the condensation of the DNA strands, which consists of a change in the conformation of its well-known B-shape. Bearing this in mind, the hybrid liposomes prepared in this work (containing lipids and surfactant) have been used as nanocarriers of nucleic acids. Taking into account the importance of the choice of a vector for a successful gene therapy, and according to the characterization results shown previously, the binding study has only been carried out with the α value equal to 0.32 (sample C). This sample generates aqueous homogeneous solutions (PDI = 0.0686) and the size of the liposomes are sufficiently small enough to favor transfection processes.

The spectroscopic properties of the RuC1C19 surfactant permitted quantifying the binding of the metallo-liposomes to ct-DNA. A decrease in the emission intensity of Ru-liposomes was observed when the polynucleotide concentration increased. This behavior is due to an interaction between the liposomes and the nucleic acid. Results were used to estimate the binding constant (K) of the process:

$$\text{Liposome} + \text{DNA} \overset{K}{\rightleftarrows} \text{Liposome/DNA (Lipoplex)} \quad (5)$$

by using the known Pseudophase Model (or Two-State Model) [32]. Metallo-liposomes of RuC1C19 in a ct-DNA solution can be found in two different states: free in the solution and bound to the polynucleotide. According to the variation in the emission intensities observed for these nanoaggregates, their two states (free and bound) will show different

emission intensities. The dependence of the average emission intensity (EI) on the nucleic acid concentration can be written as:

$$\mathbf{EI} = \frac{\mathbf{EI_{free}} + \mathbf{EI_{bound}}\ K[DNA]}{1 + K[DNA]} \quad (6)$$

where **EI** is the total emission intensity of the Ru-based liposomes in ct-DNA solutions. $\mathbf{EI_{free}}$ and $\mathbf{EI_{bound}}$ represent the emission intensities of the free and bound metallo-liposomes, respectively.

Fluorescence spectra were run at constant DNA concentration and different total liposome concentrations. Due to these working conditions, equation 5 has to be modified. Taking into account the definition of the L/D parameter (Equation (2)) and considering the liposome concentration as the total lipid (lipid + surfactant) concentration given in g/mL, Equation (6) can be written as:

$$\mathbf{EI} = \frac{\mathbf{EI_{free}} + \mathbf{EI_{bound}}\ \mathbf{K_{app}}[Liposome]}{1 + \mathbf{K_{app}}[Liposome]} \quad (7)$$

where $\mathbf{K_{app}}$ is an apparent equilibrium constant related to the equilibrium constant **K** as is indicated in Equation (8).

$$\mathbf{K_{app}} = \frac{\mathbf{K}}{\mathbf{L/D}} \quad (8)$$

Figure 5A shows the trend observed in EI with the liposome concentration. A $\mathbf{K_{app}}$ value of 2.6×10^4 $g^{-1}mL^{-1}$ was obtained at α = 0.32 from a non-linear fit by using Equation (7). This value agrees with those obtained for metallo-liposomes formed by the double-chained RuC11C11 (or RuC19C19) and 1,2-dioleoyl-sn-glycero-3-phosphoethanolamine (DOPE) [25], confirming that the binding of the Ru-based liposomes to ct-DNA is mainly due to electrostatic interactions between the cationic head groups of the ruthenium surfactants and the phosphate groups of the nucleic acid.

The B-DNA form, the normal configuration of the polynucleotide in physiological conditions, shows a circular dichroism spectrum in the wavelength range between 200 and 300 nm; with a positive band centered at 285 nm due to stacking between nitrogen bases and a negative band centered at 242 nm due to the helicity of the double strand of the polynucleotide. A change in DNA circular dichroism spectrum indicates a variation in the secondary structure of the polynucleotide. Figure 5B shows the spectrum of ct-DNA in the presence and absence of different concentrations of liposomes. A decrease of both the positive and the negative bands at L/D values < 2 is observed at constant α values. As can be seen, the bands disappear at L/D values > 2. This behavior indicates the formation of RuC1C19 lipoplexes and a change in the DNA conformation due to the formation of such aggregates.

This conformational change was confirmed by zeta potential and size measurements. Figure 5C shows a sigmoidal change in the zeta potential from negative to positive values and with ζ = 0 at an L/D value about 5 at α = 0.32. This isoneutralization in the charge of the lipoplexes agrees with an increase in the size of these aggregates, due to an aggregation of the uncharged nanostructures provoked by the diminishing in the charge of the liposome/DNA complex. A higher liposome concentration (L/D value) provoked the condensation of the polynucleotide and, therefore, a new decrease in the size of the liposome/DNA complex.

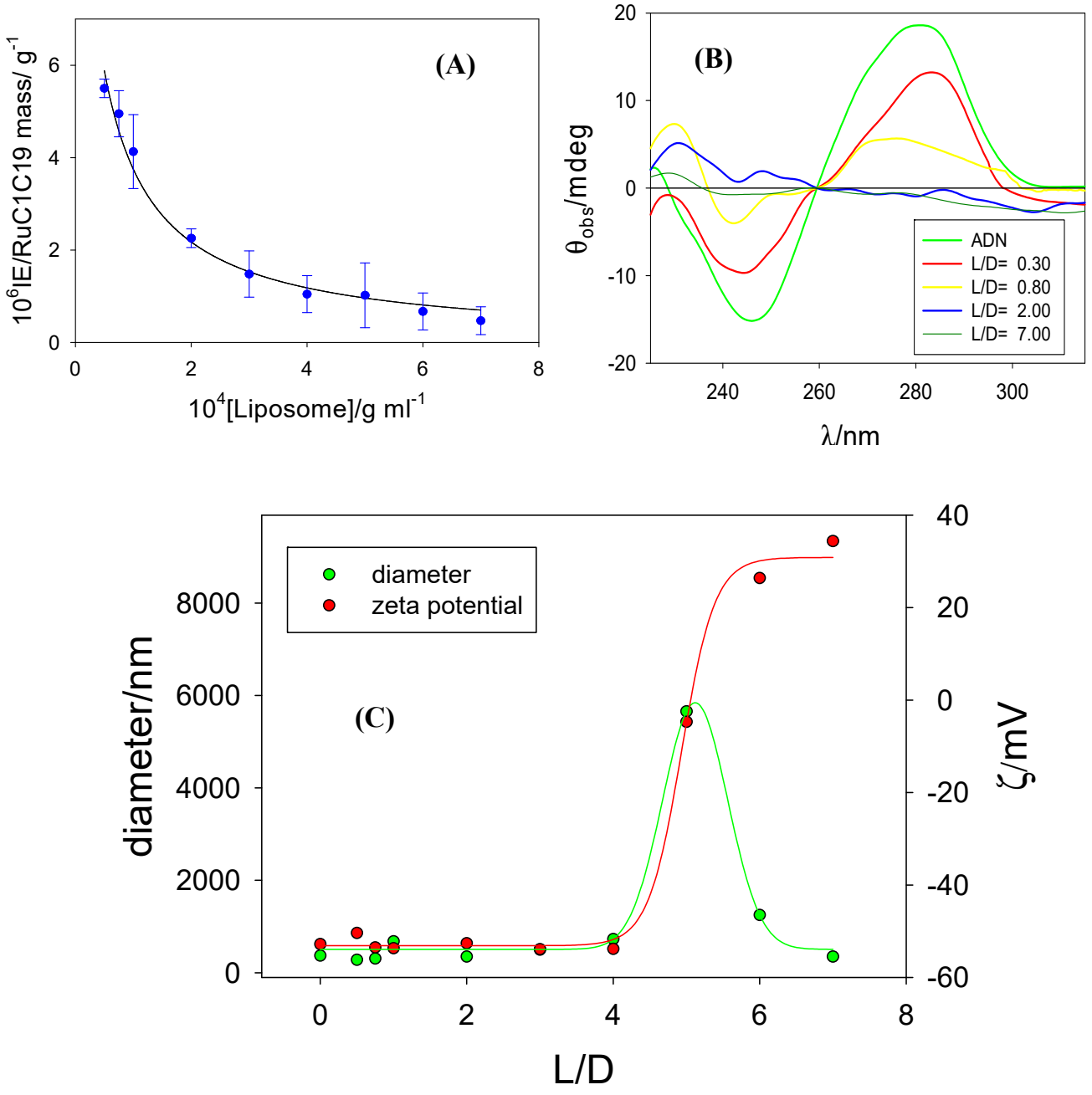

Figure 5. (**A**) Plot of EI values versus the metallo-liposomes of RuC1C19. (**B**) Circular dichroism spectra of ct-DNA at α = 0.32 and different L/D values. (**C**) Zeta potential and size data of the Ru-based lipoplexes (liposome/DNA complexes) at α = 0.32 and different L/D values.

The lipoplex sizes obtained in this work are similar to those found for liposomes containing the double-chained surfactants RuC11C11 or RuC19C19 and DOPE [25]. On the other hand, similar results are also observed with respect to the ct-DNA condensation: conformational changes in the nucleic acid happen at similar L/D ratios for a given α value, showing no dependence on the type of surfactant forming the metallo-liposomes.

Internalization and gene transfection assays were carried out at α = 0.32 and α = 0.69 values. A clear internalization process was observed in different cell lines at diverse α molar ratio (Figure 6A). Figure 6B shows the transfection process of pEGFP performed on U2OS cells. The percentage of GFP+ observed varied in the range 1–6%, slightly higher at α = 0.32 L/D = 110) than at 0.69 (L/D = 80), unimodal and bimodal populations respectively. No GFP+ was observed at lower L/D values. This percentage increased up to 8% after the

addition of DOPE, a quantity 1:1 -liposome:DOPE- (mol:mol), to the lipoplexes. However, such an addition of DOPE decreased substantially the viability of the cells. The transfection efficiency was always lower than that obtained by using Turbofect as transfection agent (close to 80%).

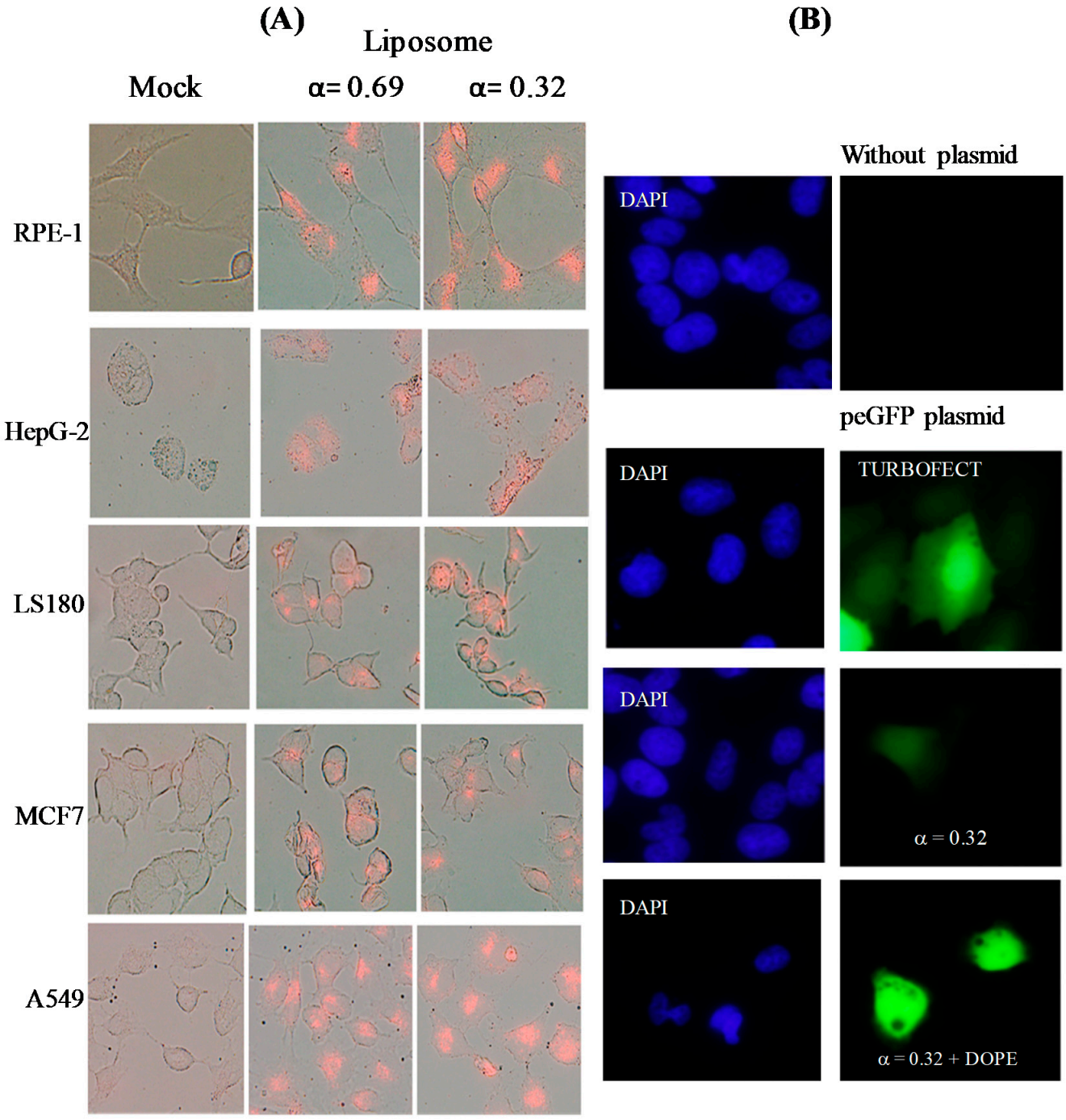

Figure 6. (**A**) Fluorescence microscopy of different cell lines in the absence (mock) and presence of liposomes at α = 0.32 and 0.69 for 24 h, washed, fixed and mounted on coverslips. Magnification 40×. (**B**) GFP expression of pEGFP in U2OS cells in the absence and presence of liposomes at α = 0.32 without and with DOPE.

3.3. Encapsulation of Doxorubicin

The structural characteristics of the liposomes enable them to act as nanocarriers of drugs. Metallo-liposomes containing the surfactant RuC1C19 and the lipids PC and CHO were used to encapsulate doxorubicin. This antibiotic is an anthracycline (see Figure 2) frequently used in the treatment of carcinomas, sarcomas and leukemia [33]. This potent antineoplastic drug has a planar structure so that it intercalates into the nitrogen base pairs of the DNA, provoking the inhibition of the Topoisomerase II activity and, therefore, avoiding the fast division of the cancer cells [34]. The use of DOX is limited due to its toxicity, causing important side-effects such as cardiotoxicity, vomiting, diarrhea and nausea [35]. These side-effects have been diminished through the encapsulation of the drug into nanocarriers such as liposomes [36,37]. The encapsulation of DOX in the metallo-liposomes of RuC1C19, PC and CHO prepared with different compositions has been studied (see Table 1).

The antibiotic was introduced into the aggregates during the hydration process of the lipid bilayer. The desired concentration of DOX solved in the buffer solution (10 mM HEPES aqueous solution, pH = 7.4) was added to the lipid bilayer, maintaining both the alternating cycles of vortex and sonication processes and the extrusion performed in the preparation of the liposomes without DOX. The DOX-loaded liposome solutions were dialyzed to calculate the antibiotic quantity encapsulated. Results are collected in Table 3.

Table 3. Encapsulation efficiency percentages (EE%) of DOX in the metallo-liposomes. Errors represent standard deviation.

SERIES	SAMPLE	α	EE%
1	**A**	0.76	76 ± 3
	B	0.43	81 ± 4
	C	0.32	93 ± 4
2	**D**	0.69	90 ± 1
	E	0.57	86 ± 5
	F	0.51	80 ± 6
3	**G**	0.65	54 ± 6
	H	0.57	88 ± 2
	I	0.37	87 ± 4

The encapsulation efficiency obtained is high for all the compositions used. As can be seen, the lowest EE% observed corresponds to sample G, which contains the highest concentrations of the surfactants RuC1C19 and PC. This behavior could be due to an electrostatic repulsion between the positive charge of the DOX, which shows a net positive charge at physiological pH conditions [38], and of the ruthenium surfactant.

In order to optimize the encapsulation process, the effect of the DOX concentration was also studied. This was only carried out with the sample C (α = 0.32); that is, the sample with the highest value for EE%. The total lipid + surfactant concentration was maintained constant in these measurements. To discuss this effect, a new parameter has to be calculated here, the loading capacity (LC), which is expressed as:

$$\mathbf{LC} = \frac{\mathbf{n_e}}{\mathbf{n_T} + \mathbf{n_L}} \times 100 \quad (9)$$

where $\mathbf{n_e}$, $\mathbf{n_T}$ and $\mathbf{n_L}$ represent the moles of encapsulated drug, total drug and total lipids, respectively.

As can be seen in Figure 7A, LC increases with the DOX concentration until reaching a constant value. The maximum loading capacity is obtained at [DOX] = 5×10^{-4} M.

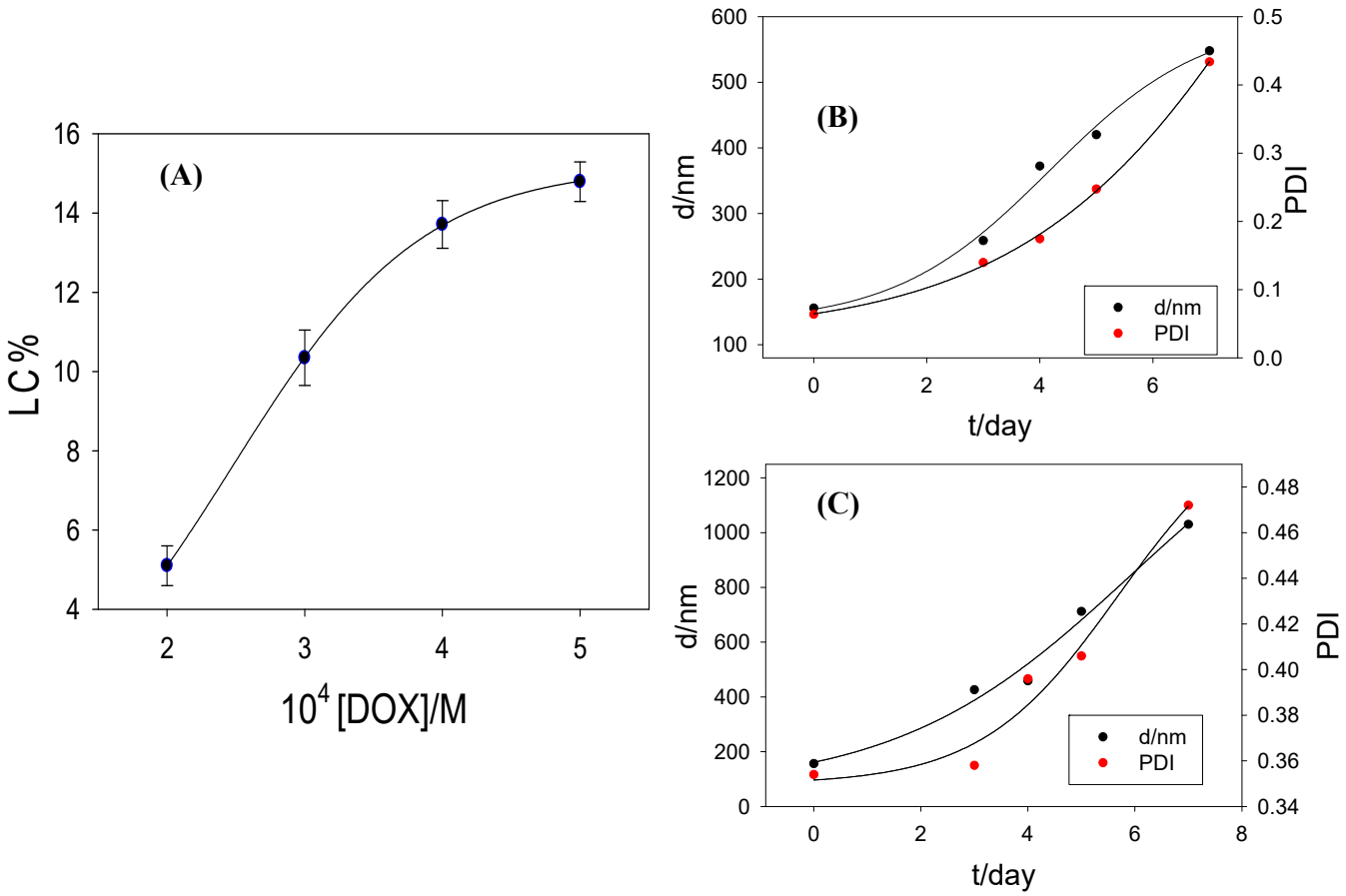

Figure 7. (**A**) Relationship of the loading capacity of DOX into RuC1C19-based metallo-liposomes with the drug concentration at $\alpha = 0.32$ and 310.1 ± 0.1 K. (**B**) Variation of the size and the polydispersity index of RuC1C19/PC/CHO liposomes with the time at $\alpha = 0.32$ at 310.1 ± 0.1 K. (**C**) Idem at $\alpha = 0.69$ at 310.1 ± 0.1 K.

An important parameter to determine in a drug-loaded nanocarrier is the release time of the pharmaceutical agent. The release of DOX could not be studied from the spectroscopic properties of the antibiotic because the liposomes of RuC1C19 absorb at a wavelength close to that corresponding to the drug, overlapping bands and leading to erroneous results. The metallo-liposomes prepared in this work are biodegradable due to the hydrolytic degradation of the phosphatidylcholine molecules in the lipid bilayer. Bearing this in mind, the release was estimated studying the degradation of the drug-loaded aggregates at the human body temperature of 310.0 ± 0.1 K in dark conditions.

The degradation process was estimated at temperatures values of 277 K and 310 K and darkness, from dynamic light scattering measurements, following the variation of both the nanoaggregate size and the polydispersity index. No variation was observed at 277 K for 7 days, so that one can be say that the liposomes are stable at least for one week when they are stored in darkness at this temperature. On the contrary, both the size and the polydispersity index increased with the time at 310 K (Figure 7B,C).

The hydrolytic destruction of the phospholipid molecules provokes the fragmentation of the lipid membrane of the liposomes and, thus, their structure will change. This variation can increase the surface area of the liposome membranes, generating an increment in the hydrodynamic radii observed from dynamic light scattering. Also, a fusion between the degraded liposomes cannot be ruled out. The decomposition of the lipid membrane can release cationic surfactant molecules from the bilayer to the solution, decreasing the charge of the liposomes and generating larger aggregates by fusion among them.

Figure 7B,C show the results of biodegradation obtained for two different α values. A gradual degradation of the nanocarriers with time is observed, as well as a total disappear-

ance of the liposome structure after 3 days. Therefore, a gradual DOX release is expected during these 3 days.

In order to know the effectivity of the encapsulated drug, a study about the effect that the encapsulated DOX causes on DNA was carried out. For this, a DOX-loaded metallo-liposome solution ($\alpha = 0.32$, [liposome] = 3×10^{-5} g/mL) was mixed with ct-DNA solutions of different concentrations (L/D = 0.07, 0.10, 0.12, 0.15, 0.22, 0.25 and 0.30). Bearing in mind that RuC1C19-based liposomes generate conformational changes in ct-DNA by themselves, as was previously discussed, L/D values lower than 0.3 were chosen in this study in order to diminish the effect of the liposomes on the polynucleotide secondary structure (see Figure 5B) and, thus, ensure the presence of DNA in its B-form. A DOX concentration of 3×10^{-5} g/mL was used and dialysis assays of the DOX-loaded liposome solutions were carried out for 12 h, previous to the addition of the polynucleotide, to eliminate the presence of non-encapsulated drug in the solution. Results show the release of DOX from the metallo-liposomes to the solution in the presence and absence of polynucleotide. This release is confirmed by the increase in the emission intensity of the DOX antibiotic observed over time (Figure 8A). The addition of ct-DNA to the drug-loaded liposome solution reduces this observed increase in emission intensity (Figure 8B). Knowing that the emission intensity of DOX decreases when the molecule is intercalated between the nitrogen base pairs of the nucleic acid, the experimental data demonstrate that the released DOX molecules from the metallo-liposomes are intercalated between the base pairs of the polynucleotide. This indicates that the released drug does not lose its effectiveness in interacting with DNA. Besides, this reveals the ability of these Ru-based liposomes to be used as drug nanocarriers.

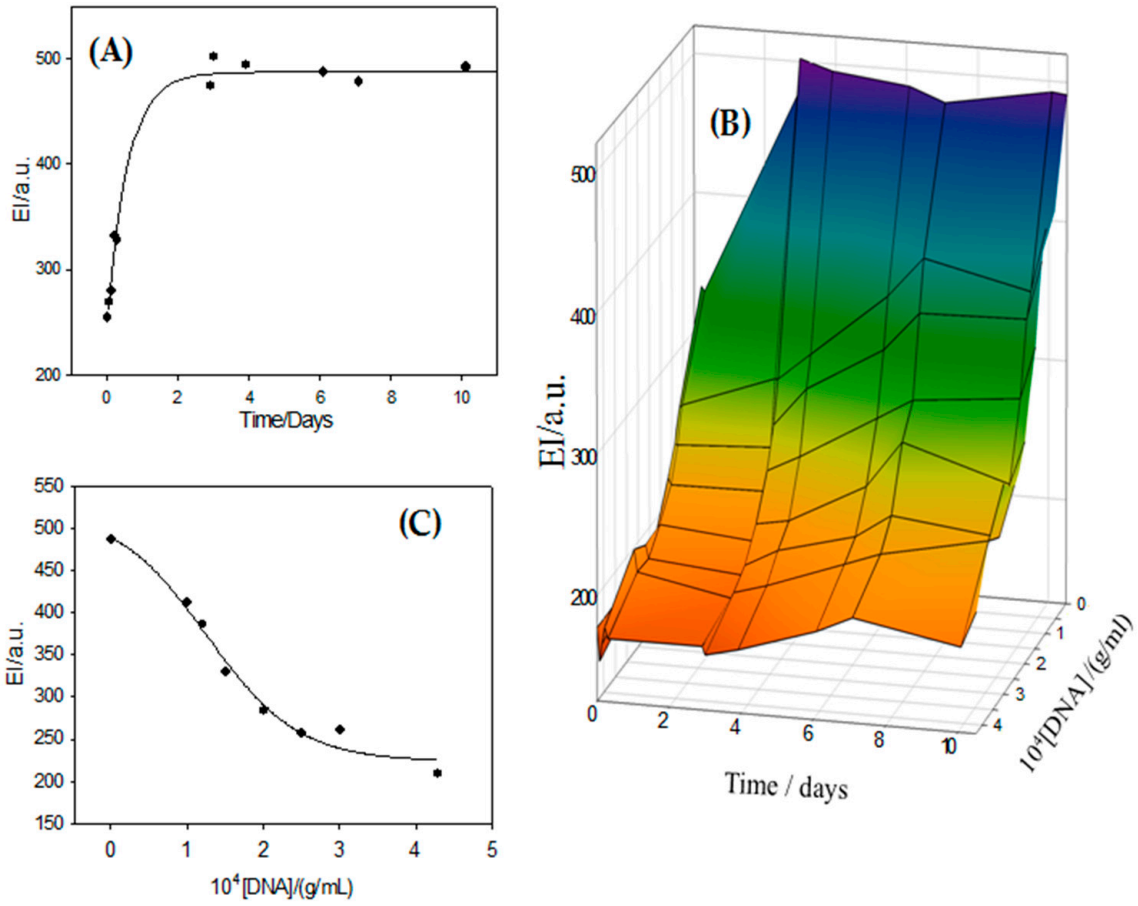

Figure 8. (**A**) Variation of the emission intensity of DOX in the ternary system liposome/DOX/ct-DNA at $\alpha = 0.32$ and [DNA] = 0 g/mL at 310.1 ± 0.1 K. (**B**) 3D-plot of DOX emission intensity versus time and ct-DNA concentration at 310.0 ± 0.1 K. (**C**) Sigmoidal dependence of EI values of DOX on the polynucleotide concentration at $\alpha = 0.32$.

The maximum EI values of DOX observed in the release process for each DNA concentration (see Figure 8B) was plotted versus the polynucleotide concentration in Figure 8C. A sigmoidal dependence was observed. This behavior demonstrates that all released DOX molecules are intercalated between the nitrogen base pairs of the nucleic acid at the highest DNA concentrations. In other words, the drug presents a strong affinity for the polynucleotide. The released drug maintains its intercalation capacity.

4. Conclusions

Cationic metallo-liposomes containing PC, CHO and RuC1C19 were prepared varying the masses of both the lipids and the surfactant. Unimodal and bimodal populations were obtained depending on the mole ratio used. Cholesterol favors the compaction of the lipid bilayer forming small liposomes and unimodal populations. TEM images showed the spherical structure of these nanoaggregates. A certain specificity of the nanoaggregates by some cell line was seen. In general, the metallo-liposomes were less toxic for the cancer cells HepG2 and U2OS, and for the normal cell line RPE-1.

The formation of the lipoplexes liposome/ct-DNA has been studied and its binding constant estimated. The own liposome was used as a biosensor due the luminescence properties of the $[Ru(bpy)_3]^{2+}$ -based surfactant. Changes in the circular dichroism spectra of the nucleic acid in the presence of the liposomes demonstrated a polynucleotide condensation at L/D values higher than 5. A good internalization of the metallo-liposomes into cancer and normal cell lines was observed. Again, the luminescence properties of these nanoaggregates allowed to carry out these measurements without the addition of another fluorescence agent, which could provoke changes in the biosystem studied. Transfection viability of about 1–6% was obtained in the U2OS cell line, somewhat higher for unimodal populations than for the bimodal ones. A comparison between different populations of metallo-aggregates has not been made previously. These results encourage us to continue working with these nanosystems. Their optimization could lead to interesting results.

Author Contributions: Conceptualization and methodology, J.A.L., M.L.-L. and P.L.-C.; software, J.A.L., I.M. and D.G.; validation, F.J.O. and J.A.L.; formal analysis, M.L.M. and P.L.-C.; investigation, all researchers; resources, I.M. and D.G.; writing—original draft preparation, P.L.-C.; writing—review J.A.L., F.J.O., M.L.-L., M.L.M. and P.L.-C.; and editing, P.L.-C.; visualization, J.A.L., F.J.O., M.L.-L., M.L.M., P.L.-C. and P.M.-G.; supervision, F.J.O., M.L.-L., and P.L.-C.; project administration, M.L.M., I.V.R. and P.L.-C.; funding acquisition, M.L.M., I.V.R. and P.L.-C. All authors have read and agreed to the published version of the manuscript.

Funding: This research was funded by the Ayudas a Consolidación de Grupos de la Junta de Andalucía (2019/FQM-206 and 2019/FQM-274) and the European Union (FEDER Funds). IVR's lab is recipient of a Ramón y Cajal Contract RYC2015-18670, and supported by grants RTI2018-100692-B-I00, PI-0005-2018 and P18-RT-1271.

Institutional Review Board Statement: Not applicable.

Informed Consent Statement: Not applicable.

Data Availability Statement: Not applicable.

Acknowledgments: Authors thank CITIUS staff (characterization and microscopy) for their efforts and assistance.

Conflicts of Interest: The authors declare no conflict of interest.

References

1. Parera, E.; Marín-García, M.; Pons, R.; Comelles, F.; Suades, J.; Barnadas Rodríguez, R. Supramolecular arrangement of molybdenum carbonyl metallosurfactants with CO-releasing properties. *Organometallics* **2016**, *35*, 484–493. [CrossRef]
2. Owen, T.; Butler, A. Metallosurfactants of bioinorganic interest: Coordination induced self-assembly. *Coord. Chem. Rev.* **2011**, *225*, 678–687. [CrossRef] [PubMed]
3. Garg, P.; Kaur, G.; Sharma, B.; Chaudhary, G.R. Fluorescein–metal hybrid surfactant conjugates as a smart material for antimicrobial photodynamic therapy against Staphylococcus aureus. *ACS Appl. Biol. Mater.* **2020**, *3*, 4674–4683. [CrossRef]

4. Marín-García, M.; Benseny-Cases, N.; Camacho, M.; Perrie, Y.; Suades, J.; Barnadas-Rodríguez, R. Metallosomes for biomedical applications by mixing molybdenum carbonyl metallosurfactants and phospholipids. *Dalton Trans.* **2018**, *47*, 14293–14303. [CrossRef]
5. Wagay, T.A.; Charingia, A.; Sutin, S.; Askari, H. Aggregation and adsorption properties of benzyldimethylhexadecylammonium tetrachloromanganate(II) metallosurfactant in water–ethylene glycol medium. *J. Disper. Sci. Technol.* **2020**, *27*, 1–10. [CrossRef]
6. Ahmad, T.; Askari, H.; Ismail, K. Synthesis, aggregation and adsorption behavior of benzyldimethylhexadecylammonium based double-chained metallosurfactants. *J. Mol. Liq.* **2020**, *299*, 112234.
7. Kaur, N.; Dhairwal, P.; Brar, A.; Kaur, G.; Bhalla, A.; Prakash, C.; Chaudhary, G.R. Amphiphilic metallosurfactants as potential scaffolds for facile fabrication of PdO-NiO nanocomposites for environmentally benign synthesis of xanthene derivatives. *Mater. Today Chem.* **2019**, *14*, 100194. [CrossRef]
8. Dogra, V.; Kaur, G.; Jindal, S.; Kumar, R.; Kumar, S.; Singhal, N.K. Bactericidal effects of metallosurfactants based cobalt oxide/hydroxide nanoparticles against Staphylococcus aureus. *Sci. Total Environ.* **2019**, *681*, 350–364. [CrossRef]
9. Sharma, B.; Kaur, G.; Chaudhay, G.R.; Gawali, S.L.; Hassan, P.A. High antimicrobial photodynamic activity of photosensitizer encapsulated dual-functional metallocatanionic vesicles against drug-resistant bacteria *S. aureus*. *Biomater. Sci.* **2020**, *8*, 2905–2920. [CrossRef]
10. Mitchell, N.; Kalber, T.L.; Cooper, M.S.; Sunassee, K.; Chalker, S.L.; Shaw, K.P.; Ordidge, K.L.; Badar, A.; Janes, S.M.; Blower, P.J.; et al. Incorporation of paramagnetic, fluorescent and PET/SPECT contrast agents into liposomes for multimodal imaging. *Biomaterials* **2013**, *34*, 1179–1192. [CrossRef]
11. Bera, S.; Chowdhury, A.; Sarkar, K.; Dastidar, P. Design and synthesis of Zn^{II}-coordination polymers anchored with NSAIDs: Metallovesicle formation and multi-drug delivery. *Chem. Asian J.* **2020**, *15*, 503–510. [CrossRef]
12. Dan, N. Vesicle-based drug carriers: Liposomes, polymersomes, and niosomes. In *Design and Development of New Nanocarriers*; Grumezescu, A.M., Ed.; William Andrew Publishing: Burlington, MA, USA, 2018; Chapter 1; pp. 1–55.
13. Hu, X.-Y.; Gao, L.; Mosel, S.; Ehlers, M.; Zellermann, E.; Jiang, H.; Knauer, S.K.; Wang, L.; Schmuck, C. From Supramolecular Vesicles to Micelles: Controllable construction of tumor-targeting nanocarriers based on host-guest interaction between a pillar[5]arene-based prodrug and a RGD-sulfonate guest. *Small* **2018**, *14*, e1803952. [CrossRef]
14. Chamundeeswari, M.; Jeslin, J.; Verma, M.L. Nanocarriers for drug delivery applications. *Environ. Chem. Lett.* **2018**, *17*, 849–865. [CrossRef]
15. Moyá, M.L.; López-López, M.; Lebrón, J.A.; Ostos, F.J.; Pérez, D.; Camacho, V.; Beck, I.; Merino-Bohórquez, V.; Cameán, M.; Madinabeitia, N.; et al. Preparation and Characterization of New Liposomes. Bactericidal Activity of Cefepime Encapsulated into Cationic Liposomes. *Pharmaceutics* **2019**, *11*, 69. [CrossRef] [PubMed]
16. Bar-Zeev, M.; Assaraf, Y.G.; Livney, Y.D. β-casein nanovehicles for oral delivery of chemotherapeutic drug combinations overcoming P-glycoprotein-mediated multidrug resistance in human gastric cancer cells. *Oncotarget* **2016**, *7*, 23322–23334. [CrossRef]
17. Hwang, S.; Lee, J.H.; Park, C.; Lee, H.; Kim, C.; Park, C.; Lee, M.-H.; Lee, W.; Park, J.; Kim, K.; et al. A highly efficient organic sensitizer for dye-sensitized solar cells. *Chem. Commun.* **2007**, *46*, 4887–4889. [CrossRef]
18. Devi, R.S.; Kumaraguru, N. Interaction of CT-DNA with Ruthenium(II) Metallosurfactant Complexes: Synthesis, CMC Determination, Antitumour and Antimicrobial Activities. *Asian J. Chem.* **2020**, *32*, 665–677. [CrossRef]
19. Garg, P.; Kaur, G.; Chaudhary, G.R.; Kaur, S.; Gawali, S.L.; Hassan, P.A. Investigating the structural integrity of Bovine serum albumin in presence of newly synthesized metallosurfactants. *Colloids Surf. B* **2018**, *164*, 116–124. [CrossRef]
20. Kashapov, R.; Razuvayeva, Y.; Ziganshina, A.; Sergeeva, T.; Lukashenko, S.; Sapunova, A.; Voloshina, A.; Kashapova, N.; Nizameev, I.; Salnikov, V.; et al. Supra-amphiphilic systems based on metallosurfactant and calix[4]resorcinol: Self-assembly and drug delivery potential. *Inorg. Chem.* **2020**, *59*, 18276–18286. [CrossRef]
21. Wei, Y.; Wang, L.; Huang, J.; Zha, J.; Yan, Y. Multifunctional metallo-organic vesicles displaying aggregation-induced emission: Two-photon cell-imaging, drug delivery and specific detection of zinc ion. *ACS Appl. Nano Mater.* **2018**, *1*, 1819–1827. [CrossRef]
22. Arroyo, I.Z.; Gomez, C.; Alarcón, H.; Jiménez, A.; Pardo, A.; Montaño, G.; Armijos, R.X.; Noveron, J.C. Alkyl Length Effects on the DNA Transport Properties of Cu (II) and Zn(II) Metallovesicles: An In Vitro and In Vivo Study. *J. Drug Deliv.* **2018**, *2018*, 1–11. [CrossRef]
23. Pal, S.; Islam, M.T.; Moore, J.T.; Reyes, J.; Pardo, A.; Valera-Ramirez, A.; Noveron, J.C. Self-assembly of a Novel Cu(II) Coordination Complex Forms Metallo-Vesicles that are able to Transfect Mammalian Cells. *New J. Chem.* **2017**, *41*, 11230–11237. [CrossRef]
24. Cruz-Campa, I.; Arzola, A.; Santiago, L.; Parsons, J.G.; Valera-Ramirez, A.; Aguilera, R.J.; Noveron, J.C. A novel class of metal-directed supramolecular DNA-delivery systems. *Chem. Commun.* **2007**, *28*, 2944–2946. [CrossRef]
25. Lebrón, J.A.; Ostos, F.J.; López-López, M.; Moyá, M.L.; Sales, C.; García, E.; García-Calderón, C.B.; García-Calderón, M.; Peña-Gómez, M.J.; Rosado, I.V.; et al. Metallo-liposomes of ruthenium used as promising vectors of genetic material. *Pharmaceutics* **2020**, *12*, 482. [CrossRef] [PubMed]
26. Zhang, X.; Zong, W.; Wang, J.; Dong, M.; Cheng, W.; Sun, T.; Han, X. Multicompartmentalized vesosomes containing DOX loaded liposomes and 5FU loaded liposomes for synergistic tumor treatment. *New J. Chem.* **2019**, *43*, 4895–4899. [CrossRef]
27. Español, L.; Larrea, A.; Andreu, V.; Mendoza, G.; Arruebo, M.; Sebastian, V.; Aurora-Prado, M.S.; Kedor-Hackmann, E.R.M.; Santoro, M.I.R.M.; Santamaria, J. Dual encapsulation of hydrophobic and hydrophilic drugs in PLGA nanoparticles by a single-step method: Drug delivery and cytotoxicity assays. *RSC Adv.* **2016**, *6*, 111060–111069. [CrossRef]

28. Wu, D.; Pusuluri, A.; Vogus, D.; Krishnan, V.; Shields IV, C.W.; Kim, J.; Razmi, A.; Mitragotri, S. Design principles of drug combinations for chemotherapy. *J. Control. Release* **2020**, *323*, 36–46. [CrossRef]
29. Kostova, I. Ruthenium Complexes as Anticancer Agents. *Curr. Med. Chem.* **2006**, *13*, 1085–1107. [CrossRef] [PubMed]
30. Süss-Fink, G. Arene ruthenium complexes as anticancer agents. *Dalton Trans.* **2010**, *7*, 1673–1688. [CrossRef]
31. Lebrón, J.A.; Ostos, F.J.; López-López, M.; Moyá, M.L.; Kardell, O.; Sánchez, A.; Carrasco, C.J.; García-Calderón, M.; García-Calderón, C.B.; Rosado, I.V.; et al. Preparation and characterization of metallomicelles of Ru(II). Cytotoxic activity and use as vector. *Colloids Surf. B.* **2019**, *175*, 116–125. [CrossRef]
32. Menger, F.M.; Portnoy, C.E. Chemistry of reactions proceeding inside molecular aggregates. *J. Am. Chem. Soc.* **1967**, *89*, 4698–4703. [CrossRef]
33. Carvalho, C.; Santos, R.; Cardoso, S.; Correia, S.; Oliveira, P.; Santos, M.; Moreira, P. Doxorubicin: The good, the bad and the ugly effect. *Curr. Med. Chem.* **2009**, *16*, 3267–3285. [CrossRef] [PubMed]
34. Ostos, F.J.; Lebrón, J.A.; Moyá, M.L.; López-López, M.; Sánchez, A.; Clavero, A.; García-Calderón, C.B.; Rosado, I.V.; López-Cornejo, P. p-Sulfocalix[6]arene as nanocarrier for controlled delivery of doxorubicin. *Chem. Asian J.* **2017**, *12*, 679–689. [CrossRef] [PubMed]
35. Thirumaran, R.; Prendergast, G.C.; Gilman, P.B. Cytotoxic chemotherapy in clinical treatment of cancer. In *Cancer Immunotherapy*; Prendergast, G.C., Jaffee, E.M., Eds.; Academic Press: Chicago, IL, USA, 2007; Chapter 7; pp. 101–116.
36. Storm, G.; van Bloois, L.; Steerenberg, P.A.; van Etten, E.; de Groot, G.; Crommelin, D.J.A. Liposome encapsulation of doxorubicin: Pharmaceutical and therapeutic aspects. *J. Control. Release* **1989**, *9*, 215–229. [CrossRef]
37. Gokhale, P.C.; Radhakrishnan, B.; Husain, S.R.; Abernethy, D.R.; Sacher, R.; Dritschilo, A.; Rahman, A. An improved method of encapsulation of doxorubicin in liposomes: Pharmacological, toxicological and therapeutic evaluation. *Br. J. Cancer* **1996**, *74*, 43–48. [CrossRef] [PubMed]
38. Feng, S.; Zhang, H.; Zhi, C.; Gao, X.-D.; Nakanishi, H. pH-responsive charge-reversal polymerfunctionalized boron nitride nanospheres for intracellular doxorubicin delivery. *Int. J. Nanomed.* **2018**, *13*, 641–652. [CrossRef]